Supporting Information

Weiss et al. 10.1073/pnas.1403500111

SI Text

Here we (*i*) provide a formal derivation of the mapping of brittle compressive failure onto the depinning transition of an elastic manifold and (*ii*) present the characteristics and the simulation settings of the discrete-element model of frictional granular media.

Brittle Compressive Failure as a Depinning Transition

We consider a scalar field representing at a mesoscopic scale the damage in a geomaterial or the plastic strain in an amorphous material or a granular material. In quasi-static loading conditions, a simple and natural way of accounting for the nonlinear nature of the mechanisms that locally induce an irreversible change of structure consists of modeling its onset by threshold dynamics on the local stress state. Damage or plasticity occurs whenever the stress state $\boldsymbol{\sigma}$ reaches the boundary of an elastic domain defined by $F(\boldsymbol{\sigma})=\sigma_c$. The heterogeneous nature of the material is accounted for by a statistical variability of the threshold σ_c.

The associated interplay between local disorder and elasticity is the basis of depinning models that have proved successful in recent years to describe various physical and mechanical phenomena. In all cases the modeling consists of reducing the problem to the motion of an elastic line (or manifold) in a random landscape. Let us denote $h(r,t)$ the location of the elastic line at time t. A general formulation of the equation of evolution in the framework of a depinning model thus reads (1)

$$\mathsf{M}\frac{\partial h}{\partial t}(\mathbf{r},t)=F_{\mathrm{ext}}(t)+\int d\mathbf{r}'J(\mathbf{r}-\mathbf{r}')[h(\mathbf{r}',t)-h(\mathbf{r},t)]+\eta[\mathbf{r},h(\mathbf{r},t)], \quad \textbf{[S1]}$$

where F_{ext} corresponds to an external driving force applied to the elastic line, M is a mobility coefficient, and η is a random noise characterized by its distribution and its spatial correlation accounting for the random nature of the material. The integral term is an elastic-like kernel depending of the phenomenon under study. The competition between elasticity and disorder in that framework is shown to induce a dynamic phase transition. Below some critical threshold, the elastic manifold advances only a finite distance before arresting. Above the threshold it can advance indefinitely and acquires a finite velocity. Close to the threshold typical critical features are recovered: divergence of a correlation length, finite size effects, etc. The application of this formalism has recently proved extremely useful in the field of solid mechanics. Models of interfacial crack propagation in mode I based on the early works of Gao and Rice (2) have enabled, for instance, the prediction of statistics of crack arrest lengths in indentation experiments (3) or the quantitative estimate of effective toughness of heterogeneous interfaces (4).

Here we propose to extend the depinning formalism to the case of compressive damage. As a starting point we discuss a model recently developed to describe plasticity of amorphous materials at a mesoscopic scale (5). In amorphous or disordered materials the development of plasticity or damage can be described as a series of local inelastic events (structural rearrangements or microcracks, respectively). In the first case, a local plastic strain ε_p can be associated to the mesoscale region where the rearrangement(s) has taken place; in the second case, a local damage D can represent the elastic weakening induced by the microcracks at the mesoscale. In both cases the occurrence of an event can be associated to the satisfaction of a criterion based on the value of the local stress field $F(\boldsymbol{\sigma})=\sigma_c$, where the random nature of σ_c accounts for the material disorder. In both cases, the occurrence of a local inelastic event in an elastic matrix (the remainder of the material) is responsible for an internal stress field. The modeling of this internal stress field is a key ingredient in the development of the model.

The internal stress field induced by an inelastic event can obviously be computed numerically as detailed below in *Discrete-Element Model of Frictional Granular Media*. It will depend on the fine details of the inelastic event as well as the elastic matrix. However, far from the rearrangement only the asymptotic far field will really matter. In the present framework of building a depinning model at mesoscopic scale, we concentrate on the asymptotic far field and forget about the finer details.

In two of the most influential papers ever published in solid mechanics, Eshelby calculated the stress field induced by an ellipsoidal inclusion (6, 7). It appears that in the far field the elastic interaction scales as r^{-d}, where r is the distance and d the topological dimension. This interaction exhibits an anisotropic character: In some directions the stress is enhanced whereas in others it is decreased. This anisotropy of the elastic interaction is a key ingredient of the modeling of the localization behavior in amorphous plasticity as in damage. More specifically, Eshelby solved two different inclusion problems. The first one, also known as the eigenstrain problem, consists of finding the elastic stress induced by a deformed inclusion in an elastic matrix. In this case both inclusion and matrix are made of the same material. This case naturally applies to an inclusion that has undergone plastic deformation. It also applies, with some simplifying assumptions, to the case of granular media undergoing irreversible local rearrangements of the granular structure (*Discrete-Element Model of Frictional Granular Media*). The second problem, known as the inhomogeneity problem, consists of finding the elastic stress induced in an elastic matrix under remote loading by an inclusion characterized by elastic properties different from those of the matrix. This case applies to an inclusion that has undergone local damage.

Plastic Inclusions and Amorphous Plasticity. For the sake of simplicity we restrict to the case of a 2D problem (e.g., plane strain). In the absence of inclusion we consider a biaxial loading characterized by σ_x^{ext} and σ_y^{ext}. The material is characterized by a Young modulus E and a Poisson coefficient υ. Let us now consider a unique circular inclusion of radius λ. The inclusion is located at the origin and polar coordinates are used.

We first specialize to the case of plasticity (the first Eshelby problem). The inclusion has undergone plastic deformation that in absence of the matrix would result in a local plastic (purely deviatoric) strain ε_p. Assuming that the symmetry of this local plastic strain is the same as the external loading, we obtain for the elastic perturbation (e.g., ref. 8)

$$\begin{aligned}\sigma_{xx}-\sigma_{yy}&=\Lambda\frac{E}{1-\upsilon^2}\frac{\lambda^2\langle\varepsilon_p\rangle\cos(4\theta)}{r^2}\\ \sigma_{xy}&=\Lambda\frac{E}{1-\upsilon^2}\frac{\lambda^2\langle\varepsilon_p\rangle\sin(4\theta)}{r^2}\\ \sigma_{xx}+\sigma_{yy}&=\Lambda\frac{E}{1-\upsilon^2}\frac{\lambda^2\langle\varepsilon_p\rangle\cos(2\theta)}{r^2},\end{aligned} \quad \textbf{[S2]}$$

where Λ is a constant depending on υ. A crucial point here is that whatever the precise shape of the reorganized region is, the far-field asymptotics will remain unchanged, with an amplitude proportional to the surface $S=\pi\lambda^2$ of an equivalent spherical inclusion times the mean plastic deformation ε_p it would have undergone in the absence of a surrounding matrix.

Note here another crucial point: In this first case of amorphous plasticity, matrix and inclusion are characterized by the same elastic properties. The case of multiple inclusions is thus immediately solved by superposition.

In this framework, assuming a scalar plastic criterion based on the sole local shear stress $\tau = |\sigma_{xx} - \sigma_{yy}|$, a simple equation of evolution for the plastic strain ε_p can be written in the framework of a quasi-static loading, considering an overdamped dynamics (5)

$$\mathsf{M}\frac{\partial \varepsilon_p(\mathbf{r},t)}{\partial t} = \mathcal{R}\left[\tau^{\rm ext}(t) + \tau^{\rm el}\left(\mathbf{r},\{\varepsilon_p\}\right) - \tau_c\left(\mathbf{r},\varepsilon_p\right)\right], \qquad \textbf{[S3]}$$

where $\mathcal{R}$ denotes the positive part, and

$$\tau^{\rm el}\left(\mathbf{r},\{\varepsilon_p\}\right) = A\int \frac{\cos(4\theta_{rr'})}{|\mathbf{r}-\mathbf{r}'|^2}\left[\varepsilon_p(\mathbf{r}',t) - \varepsilon_p(\mathbf{r},t)\right]d\mathbf{r}'. \qquad \textbf{[S4]}$$

One recovers here a typical depinning model, consistent with the general definition given above in **[S1]** with an external driving "force" $\tau^{\rm ext}$, a random field τ_c, and an elastic kernel $\tau^{\rm el}$. Note here that in contrast to most depinning models, the elastic kernel is anisotropic, which induces a specific localization behavior to the model (5). To complete the depinning interpretation we can embed the 2D lattice in a 3D space where the extra coordinate is given by the plastic strain ε_p. In so doing we recover the motion of a 2D manifold in a 3D random landscape.

Compressive Damage: From Elastic Inhomogeneities to Stress Fluctuations. We discuss now the case of a circular inhomogeneity of radius λ, of Young modulus $E_1 = E_0(1-D)$, where D is the local damage, and (for the sake of simplicity) of unchanged Poisson coefficient υ. In plane strain we note $\kappa = 3\text{–}4\upsilon$. We consider a remote biaxial stress characterized by $\sigma_x^{\rm ext}$ and $\sigma_y^{\rm ext}$. The far-field internal stress induced by the inhomogeneity reads

$$\begin{aligned}
\sigma_{xx}+\sigma_{yy} &= \frac{-2D}{1+\kappa(1-D)}\,\frac{\lambda^2\left(\sigma_x^{\rm ext}-\sigma_y^{\rm ext}\right)\cos(2\theta)}{r^2}\\
\sigma_{xx}-\sigma_{yy} &= \frac{-2D}{1+\kappa(1-D)}\,\frac{\lambda^2\left(\sigma_x^{\rm ext}-\sigma_y^{\rm ext}\right)\cos(4\theta)}{r^2}\\
&\quad + \frac{1}{2}\,\frac{D}{1+2(1-D)/(\kappa-1)}\,\frac{\lambda^2\left(\sigma_x^{\rm ext}+\sigma_y^{\rm ext}\right)\cos(2\theta)}{r^2}\\
\sigma_{xy} &= \frac{-D}{1+\kappa(1-D)}\,\frac{\lambda^2\left(\sigma_x^{\rm ext}-\sigma_y^{\rm ext}\right)\sin(4\theta)}{r^2}\\
&\quad + \frac{1}{4}\,\frac{D}{1+2(1-D)/(\kappa-1)}\,\frac{\lambda^2\left(\sigma_x^{\rm ext}+\sigma_y^{\rm ext}\right)\sin(2\theta)}{r^2}.
\end{aligned} \qquad \textbf{[S5]}$$

This gives in a more condensed form

$$\begin{aligned}
\sigma_{xx}+\sigma_{yy} &= \left(\sigma_x^{\rm ext}-\sigma_y^{\rm ext}\right)f(D)B_2\left(\frac{r}{\lambda},\theta\right)\\
\sigma_{xx}-\sigma_{yy} &= \left(\sigma_x^{\rm ext}-\sigma_y^{\rm ext}\right)f(D)B_4\left(\frac{r}{\lambda},\theta\right) + \left(\sigma_x^{\rm ext}+\sigma_y^{\rm ext}\right)g(D)B_2\left(\frac{r}{\lambda},\theta\right)\\
\sigma_{xy} &= \frac{1}{2}\left(\sigma_x^{\rm ext}-\sigma_y^{\rm ext}\right)f(D)C_4\left(\frac{r}{\lambda},\theta\right)\\
&\quad + \frac{1}{2}\left(\sigma_x^{\rm ext}+\sigma_y^{\rm ext}\right)g(D)C_2\left(\frac{r}{\lambda},\theta\right),
\end{aligned} \qquad \textbf{[S6]}$$

where the functions B and C present an inverse quadratic dependence with distance and the indexes 2 and 4 denote the dipolar and quadrupolar symmetries, respectively. Note that for small values of D, functions f and g can be regarded as almost linear.

How do we extend this result, obtained with an isolated inhomogeneity, to the stress induced by a damage field $D(\mathbf{r})$? The disordered material can be here regarded as a set of inhomogeneities of size λ, the discretization scale of the model. In contrast to the case of plasticity, the generalization to a large number of inhomogeneities is not immediate because of interactions between them and so simple superposition is not exact here. Our approximation consists of considering that the internal stress field results from a superposition of the stresses induced by individual inclusions embedded in an equivalent matrix of effective modulus (at the macroscale) $\overline{E} = E_0(1-\overline{D})$, where E_0 is the initial Young modulus of the material and $\overline{D}$ is the effective mean damage.

Before detailing our approach, it is of interest to briefly discuss the question of the elastic behavior of disordered materials and its implication for damage. Historically, mechanical engineering studies have focused on homogenization, i.e., the determination of the average elastic properties at a macroscopic scale from the knowledge of the microscopic properties. Conversely, statistical physics studies mainly focused on the stress fluctuations induced by the elastic disorder. Here we consider the evolution with damage of both the mean elastic behavior and its fluctuations.

Consider the material at a given stage of damage. The damage field $D(\mathbf{r})$ gives immediate access to the heterogeneous elastic properties, $E(\mathbf{r}) = E_0[1-D(\mathbf{r})]$. Here and in the following (for the sake of simplicity) the Poisson coefficient ν is assumed to remain unchanged. From this knowledge, an effective (average) Young modulus $\overline{E}$ can be defined at a macroscopic scale. A fluctuating damage field $D^{\rm fluc}(\mathbf{r})$ can thus be defined from the contrast between the actual elastic moduli at a microscopic scale $E(\mathbf{r})$ and the effective (average) modulus $\overline{E}$ at a macroscopic scale. Stress fluctuations can be then obtained from this fluctuating damage field.

What is the effect of the occurrence of a localized damage event in this framework? At first it will affect (weaken) the average elastic behavior: Effective moduli will undergo a slight decrease. As a direct consequence of this evolution of the average elastic behavior, stress fluctuations induced by the stiffer (less damaged than average) regions will be amplified because the contrast with the effective matrix has increased. Conversely, stress fluctuations induced by the softer (more damaged than average) regions will be attenuated. On top of that, the newly damaged area will give an additional contribution to the stress fluctuations.

This sets the theoretical framework of our approach. No particular approximation has been performed so far because the methods to be used for the determination of the effective modulus $\overline{E}$ and the stress fluctuations remain to be specified. Note in particular that interactions between inhomogeneities can affect the determination of both the effective moduli and the stress fluctuations. To be more specific and make possible a future numerical implementation (out of the scope of the present study), a natural choice would consist of resorting to a self-consistent approximation for the computation of the effective modulus $\overline{E}$ and to a simple superposition of isolated inhomogeneities within the just-defined effective matrix to compute the stress fluctuations. In so doing the internal stress is thus obtained through two successive steps: (*i*) the determination of the Young modulus $\overline{E}$ of the effective matrix associated to a given damage field $D(\mathbf{r})$ and (*ii*) the computation of the stress fluctuations from isolated "effective" inhomogeneities due to the contrast between the local moduli $E(r)$ and the effective modulus $\overline{E}$. Here the self-consistent scheme proposed for step *i* partly accounts for interactions between inhomogeneities whereas for step *ii* these interactions are not explicitly accounted for, but only via the value of the effective modulus $\overline{E}$ that sets the precise level of elastic contrast of each inhomogeneity.

Using the effective mean damage $\overline{D}$ that derives from the self-consistent estimate of the effective modulus $\overline{E} = E_0(1-\overline{D})$, we define the fluctuating damage field $D^{\mathrm{fluc}}(\mathbf{r})$ that gives the local contrast to the effective matrix:

$$D^{\mathrm{fluc}}(\mathbf{r}) = \frac{D(\mathbf{r}) - \overline{D}}{1 - \overline{D}}. \qquad \textbf{[S7]}$$

We can now write the internal stress induced by the damage field $D(\mathbf{r})$ as a superposition of the stress fields radiated by the local inhomogeneities $D^{\mathrm{fluc}}(\mathbf{r})$ within the homogeneous matrix of modulus $\overline{E}$:

$$\sigma_{xx}^{\mathrm{el}}(\mathbf{r}) + \sigma_{yy}^{\mathrm{el}}(\mathbf{r}) = \left(\sigma_x^{\mathrm{ext}} - \sigma_y^{\mathrm{ext}}\right) \int f\left[D^{\mathrm{fluc}}(\mathbf{r}') - D^{\mathrm{fluc}}(\mathbf{r})\right] B_2\left(\frac{|\mathbf{r}-\mathbf{r}'|}{\lambda}, \theta_{r,r'}\right) d\mathbf{r}'$$

$$\begin{aligned}\sigma_{xx}^{\mathrm{el}}(\mathbf{r}) - \sigma_{yy}^{\mathrm{el}}(\mathbf{r}) = {} & \left(\sigma_x^{\mathrm{ext}} - \sigma_y^{\mathrm{ext}}\right) \int f\left[D^{\mathrm{fluc}}(\mathbf{r}') - D^{\mathrm{fluc}}(\mathbf{r})\right] B_4\left(\frac{|\mathbf{r}-\mathbf{r}'|}{\lambda}, \theta_{r,r'}\right) d\mathbf{r}' \\ & + \left(\sigma_x^{\mathrm{ext}} + \sigma_y^{\mathrm{ext}}\right) \int g\left[D^{\mathrm{fluc}}(\mathbf{r}') - D^{\mathrm{fluc}}(\mathbf{r})\right] B_2\left(\frac{|\mathbf{r}-\mathbf{r}'|}{\lambda}, \theta_{r,r'}\right) d\mathbf{r}'\end{aligned} \qquad \textbf{[S8]}$$

$$\begin{aligned}\sigma_{xy}^{\mathrm{el}}(\mathbf{r}) = {} & \frac{1}{2}\left(\sigma_x^{\mathrm{ext}} - \sigma_y^{\mathrm{ext}}\right) \int f\left[D^{\mathrm{fluc}}(\mathbf{r}') - D^{\mathrm{fluc}}(\mathbf{r})\right] C_4\left(\frac{|\mathbf{r}-\mathbf{r}'|}{\lambda}, \theta_{r,r'}\right) d\mathbf{r}' \\ & + \frac{1}{2}\left(\sigma_x^{\mathrm{ext}} + \sigma_y^{\mathrm{ext}}\right) \int g\left[D^{\mathrm{fluc}}(\mathbf{r}') - D^{\mathrm{fluc}}(\mathbf{r})\right] C_2\left(\frac{|\mathbf{r}-\mathbf{r}'|}{\lambda}, \theta_{r,r'}\right) d\mathbf{r}'.\end{aligned}$$

Compressive Damage: Stress-Based Criterion. We use the Coulomb criterion, $|\tau| + \mu\sigma_N = \tau_C$, to define the onset of damage, with $\mu = \tan(\varphi)$ the internal friction coefficient and φ the angle of internal friction. This criterion can be rewritten as a function of the eigenvalues of the stress tensor $\sigma_1 > \sigma_2$ as (9)

$$F(\sigma) = (\sigma_1 - \sigma_2) + (\sigma_1 + \sigma_2)\sin(\varphi) - 2\cos(\varphi)\tau_C = 0. \qquad \textbf{[S9]}$$

To map this compressive damage problem onto a depinning model, we rewrite this last expression for a biaxial stress state perturbed by the elastic contributions induced by the damage field, $\sigma = \sigma^{\mathrm{ext}} + \sigma^{\mathrm{el}}$. This requires the computation of the eigenvalues σ_1 and σ_2, which are obtained from

$$\sigma_1 + \sigma_2 = \left(\sigma_x^{\mathrm{ext}} + \sigma_y^{\mathrm{ext}}\right) + \left(\sigma_{xx}^{\mathrm{el}} + \sigma_{yy}^{\mathrm{el}}\right) \qquad \textbf{[S10]}$$

and

$$(\sigma_1 - \sigma_2)^2 = \left(\sigma_x^{\mathrm{ext}} - \sigma_y^{\mathrm{ext}}\right)^2 + 2\left(\sigma_x^{\mathrm{ext}} - \sigma_y^{\mathrm{ext}}\right)\left(\sigma_{xx}^{\mathrm{el}} - \sigma_{yy}^{\mathrm{el}}\right) + \left(\sigma_1^{\mathrm{el}} - \sigma_2^{\mathrm{el}}\right)^2. \qquad \textbf{[S11]}$$

Note that we expect σ^{el} to be of the order of $\epsilon \times \sigma^{\mathrm{ext}}$, where the magnitude small parameter ϵ should be given by the typical value of damage (relative fluctuation of the elastic modulus). Restricting our calculation to first order and replacing the internal stress by a superposition of Eshelby stresses induced by effective inhomogeneities as derived above, we obtain

$$\sigma_1 + \sigma_2 = \left(\sigma_x^{\mathrm{ext}} + \sigma_y^{\mathrm{ext}}\right) + \left(\sigma_x^{\mathrm{ext}} - \sigma_y^{\mathrm{ext}}\right)\mathcal{A}_2 \qquad \textbf{[S12]}$$

and

$$\begin{aligned}(\sigma_1 - \sigma_2)^2 = {} & \left(\sigma_x^{\mathrm{ext}} - \sigma_y^{\mathrm{ext}}\right)^2 + 2\left(\sigma_x^{\mathrm{ext}} - \sigma_y^{\mathrm{ext}}\right)^2 \mathcal{B}_4 \\ & + 2\left(\sigma_x^{\mathrm{ext}} - \sigma_y^{\mathrm{ext}}\right)\left(\sigma_x^{\mathrm{ext}} + \sigma_y^{\mathrm{ext}}\right)\mathcal{B}_2 + O\left(\epsilon^2\right),\end{aligned} \qquad \textbf{[S13]}$$

which gives

$$\sigma_1 - \sigma_2 = \left(\sigma_x^{\mathrm{ext}} - \sigma_y^{\mathrm{ext}}\right)(1 + \mathcal{B}_4) + \left(\sigma_x^{\mathrm{ext}} + \sigma_y^{\mathrm{ext}}\right)\mathcal{B}_2 + O\left(\epsilon^2\right), \qquad \textbf{[S14]}$$

where

$$\mathcal{A}_2\left[\{D\}, \frac{\mathbf{r}}{\lambda}\right] = \int f\left[D^{\mathrm{fluc}}(\mathbf{r}') - D^{\mathrm{fluc}}(\mathbf{r})\right] B_2\left(\frac{|\mathbf{r}-\mathbf{r}'|}{\lambda}, \theta_{r,r'}\right) d\mathbf{r}'$$

$$\mathcal{B}_2\left[\{D\}, \frac{\mathbf{r}}{\lambda}\right] = \int g\left[D^{\mathrm{fluc}}(\mathbf{r}') - D^{\mathrm{fluc}}(\mathbf{r})\right] B_2\left(\frac{|\mathbf{r}-\mathbf{r}'|}{\lambda}, \theta_{r,r'}\right) d\mathbf{r}'$$

$$\mathcal{B}_4\left[\{D\}, \frac{\mathbf{r}}{\lambda}\right] = \int f\left[D^{\mathrm{fluc}}(\mathbf{r}') - D^{\mathrm{fluc}}(\mathbf{r})\right] B_4\left(\frac{|\mathbf{r}-\mathbf{r}'|}{\lambda}, \theta_{r,r'}\right) d\mathbf{r}'.$$

We can now rewrite the Coulomb criterion

$$\begin{aligned}F(\sigma) = {} & \left(\sigma_x^{\mathrm{ext}} - \sigma_y^{\mathrm{ext}}\right) + \left(\sigma_x^{\mathrm{ext}} + \sigma_y^{\mathrm{ext}}\right)\sin(\varphi) + \left(\sigma_x^{\mathrm{ext}} - \sigma_y^{\mathrm{ext}}\right)\mathcal{B}_4 \\ & + \left(\sigma_x^{\mathrm{ext}} + \sigma_y^{\mathrm{ext}}\right)\mathcal{B}_2 + \left(\sigma_x^{\mathrm{ext}} - \sigma_y^{\mathrm{ext}}\right)\mathcal{A}_2\sin(\varphi) - 2\cos(\varphi)\tau_C\end{aligned} \qquad \textbf{[S15]}$$

or in a more condensed way

$$F(\sigma) = \sigma_s^{\mathrm{ext}} + \sigma_s^{\mathrm{el}}\left(\{D\}, \frac{\mathbf{r}}{\lambda}\right) - 2\cos(\varphi)\tau_C(\mathbf{r}), \qquad \textbf{[S16]}$$

where $\tau_C(\mathbf{r})$ is the spatially fluctuating cohesion [note that we may have also the cohesion depending on the damage field, $\tau_C(\{D\}, \mathbf{r})$, if the disorder is not fully quenched], and

$$\sigma_s^{\mathrm{ext}} = \left(\sigma_x^{\mathrm{ext}} - \sigma_y^{\mathrm{ext}}\right) + \left(\sigma_x^{\mathrm{ext}} + \sigma_y^{\mathrm{ext}}\right)\sin(\varphi)$$

$$\begin{aligned}\sigma_s^{\mathrm{el}}\left(\{D\}, \frac{\mathbf{r}}{\lambda}\right) = {} & \left(\sigma_x^{\mathrm{ext}} - \sigma_y^{\mathrm{ext}}\right)\mathcal{B}_4\left(\{D\}, \frac{\mathbf{r}}{\lambda}\right) + \left(\sigma_x^{\mathrm{ext}} + \sigma_y^{\mathrm{ext}}\right)\mathcal{B}_2\left(\{D\}, \frac{\mathbf{r}}{\lambda}\right) \\ & + \left(\sigma_x^{\mathrm{ext}} - \sigma_y^{\mathrm{ext}}\right)\mathcal{A}_2\left(\{D\}, \frac{\mathbf{r}}{\lambda}\right)\sin(\varphi).\end{aligned}$$

Combining these expressions with **[S16]**, we can now write a simple equation of evolution of the damage field based on the positive part of the yield function $F(\sigma)$. The damaging rate is assumed to linearly depend on the excess of the local stress with respect to the Coulomb stress. As detailed above, the local stress is a sum of two contributions, the externally imposed stress and an internal stress that depends on the full damage field. We thus recover a complete mapping onto a depinning model, with the following equation of evolution of the damage field,

$$\mathsf{M}\frac{\partial D}{\partial t}(\mathbf{r}) = \mathcal{R}\left[\sigma_s^{\mathrm{ext}} + \sigma_s^{\mathrm{el}}\left(\{D\}, \overline{E}(\{D\}), \frac{\mathbf{r}}{\lambda}\right) - 2\cos(\varphi)\tau_C(\mathbf{r}, D)\right], \qquad \textbf{[S17]}$$

where $\mathcal{R}$ denotes, as above, the positive part. We identify σ_s^{ext} as the external forcing term, σ_s^{el} as the elastic contribution induced by the damage field D, and τ_C the disorder. In **[S17]**, we have made explicit the dependence of the internal stress σ_s^{el} on the modulus $\overline{E}$ of the effective elastic matrix to make more apparent the two successive steps of its computation (self-consistent estimate of the modulus of the effective matrix and superposition of the elastic interactions induced by isolated inhomogeneities within the effective matrix).

Following Eq. **S16** a stress threshold $\sigma_C = 2\tau_C \cos(\varphi)$ can be defined. The fluctuations of the local stress threshold $\delta\sigma_C = 2\delta\tau_C \cos(\varphi)$ give a natural scale for the stress fluctuations within the material. We thus expect the characteristic lengths L_A and L_B to be dressed with a parameter that depends on $\delta\sigma_C$. λ being the characteristic length scale of the disorder (i.e., the discretization scale of our mesoscopic model), we thus expect the strength fluctuations to scale as $\delta(\sigma_f)/\sigma_\infty = C(\delta\tau_c/\tau_c)(L/\lambda)^{-1/\nu_{FS}}$ and the length scales L_A and L_B as $L_{A,B} \sim \lambda(\delta\tau_c/\tau_c)^{\nu_{FS}}$. In the case of strong disorder $\delta\tau_c \gg \tau_c$ these length scales can thus be significantly larger than λ.

This description of the internal stress field induced by the progressive damage as a simple superposition of the stress fields induced by isolated inhomogeneities within an effective matrix is obviously only approximate. Two limitations may be emphasized at this stage. First, the asymptotic field cannot be reduced to the effect of an equivalent spherical inclusion and also depends on the shape (10, 11). In the presence of cracks, we expect, for instance, anisotropic effects that are not accounted for in the present modeling. In particular, the homogeneous effective matrix (used here as an intermediate step to compute the internal stress) can be anisotropic whereas it has been considered here as isotropic. Moreover, as damage is progressive, the matrix to be considered around the inclusion is itself already damaged. As proposed above, one may use an effective modulus to account for the weakening. Still an important feature will be missed: the asymmetry of the elastic properties of the damaged matrix between loading and unloading. This question has been discussed by Roux and Hild (12), who analyzed the behavior of the elastic influence function along the damage process. They show that this influence function can still be described as a power law of the distance to the crack or inclusion but with an exponent that depends on the state of damage and that eventually approaches mean-field interaction.

As already mentioned in the main text, the case of a cohesionless frictional granular medium compressed under confinement can be interpreted as an intermediate case between the amorphous plasticity and compressive damage problems. This frictional granular material may be described by Eq. **S17** derived above for the evolution of damage, replacing the damage variable D by the plastic strain variable ε_p and using for the elastic stress the same strategy as above, starting from Eq. **S2** (homogeneous Eshelby) instead of Eq. **S5** (inhomogeneous Eshelby). Numerical simulations are necessary for a complete description, as detailed in *Discrete-Element Model of Frictional Granular Media* below.

Within the approximations discussed above, amorphous plasticity as well as compressive damage can be discussed in the theoretical framework of a depinning model (Eqs. **S3** and **S17**). By construction such models exhibit a dynamical phase transition. Below a critical value of the applied external stress, the material experiences only limited damage (or plastic deformation) and its structural integrity remains. The closer the external stress is to threshold, the larger the extent of damage. Failure (or plastic flow) is eventually obtained once the critical threshold is reached. This description of mechanical failure as a critical phase transition implies the presence of traditional features of criticality, in particular the divergence of a correlation length and universal statistics of finite size effects (13–15), as detailed in the main text. In addition, the anisotropic character of the elastic kernels associated with Eshelby inclusions naturally induces a localization behavior (5).

Discrete-Element Model of Frictional Granular Media

Simulations of the mechanical behavior of granular materials were performed using the molecular dynamics discrete element method (16). The main characteristics of the model, which has been described in more detail elsewhere (17), are summarized below.

Two-dimensional granular assemblies made of a set of N_g frictional circular grains were considered. The dynamic equations are solved for each of the grains, which interact via linear elastic laws and Coulomb friction when they are in contact (18). The normal contact force f_n is related to the normal apparent interpenetration δ_n of the contacts as $f_n = k_n \times \delta_n$, where k_n is the normal contact stiffness coefficient ($\delta_n > 0$ if a contact is present, and $\delta_n = 0$ if there is no contact). The tangential component f_t of the contact force is proportional to the tangential elastic relative displacement, with a tangential stiffness coefficient k_t. Here we set $k_t = k_n$. Neither cohesion between grains nor rolling resistance is considered. The Coulomb condition $|f_t| \le \mu_{\mathrm{micro}}$, where μ_{micro} is the grain friction coefficient, requires an incremental evaluation of f_t every time step, which leads to some amount of slip each time one of the equalities $f_t = \pm\mu_{\mathrm{micro}} \times f_n$ is reached. A normal viscous component opposing the relative normal motion of any pair of grains in contact is also added to the elastic force f_n to obtain a damping of the dynamics.

All of the granular assemblies built for the present work were obtained under static loading in the absence of body forces (such as gravity). Circular 2D grains of uniformly distributed surfaces are considered. The polydispersity is kept constant for all samples, setting the largest grain diameter $D_{\max}$ such that $D_{\max} = 3D_{\min}$.

Sample Preparation. The particles are randomly (in terms of diameter) placed on sites of a regular lattice of spacing $D_{\max}$, before being mixed. This mixing procedure uses the contact dynamics (CD) method (16), so considers hard disks, and consists in setting grains in motion with random velocities, leaving them to interact in collisions that preserve kinetic energy, to produce a disordered configuration. At the end of this procedure, all grains velocities are set equal to 0 and an isotropic compression is performed using the molecular dynamics (MD) method.

This isotropic compression step of sample preparation is here performed in two different ways, and three different types of initial samples named highly coordinated (HC), low-coordinated 1 (LC1), and LC2 differing in packing fraction and coordination number are built as explained in the following. The results shown in Fig. 3 of the main text correspond to the intermediate configuration LC1.

HC samples. HC and very dense samples are obtained from an isotropic compression on frictionless grains, i.e., setting a particle friction value $\mu_{\mathrm{iso}} = 0$. The samples built in that case show values of initial packing density Φ_{ini} of the order of 0.847 ± 0.001 and a backbone coordination number, i.e., average number of contacts by grain that carry forces, $Z^*_{\mathrm{ini}} = 4$.

Initially LC samples. LC samples, characterized by Z^*_{ini} of the order of 3, are obtained following the method of ref. 18, i.e., by maintaining strongly agitated granular gas states at high densities before performing the isotropic compression with a final value of friction coefficient. Contrary to ref. 18, shaking is here performed at various distances from the maximum packing fraction (obtained from *HC samples*), by tuning the expansion parameter α. Details of the procedure, starting from a disordered granular gas, are as follows:

First, an isotropic compression is performed on frictionless particles until reaching an equilibrium state of maximum packing fraction, as done in *HC samples*).

Second, a homogeneous expansion, multiplying all coordinates by a constant factor α slightly larger than 1, is performed. Two values for α, which both lead to an expansion greater than the maximum grain interpenetration, are taken into account in this study. We considered $\alpha = 1.01$ to build samples of type LC1, which are characterized by packing densities similar to the samples obtained in *HC samples*, i.e., Φ_{ini} of the order of 0.847 ± 0.001 and $\alpha = 1.1$ to build samples of type LC2, which are characterized by smaller packing densities of $\Phi_{\mathrm{ini}} = 0.82 \pm 0.002$.

Third, a shaking procedure that uses the same contact dynamics code as the one used during the preparation of the granular gas is performed. The number of iterations n_{it} is imposed to be constant for all samples generated. Here, we set $n_{\mathrm{it}} = 5 \times 10^5$, which corresponds to the lower bound value above which the values of Φ_{ini} and Z^*_{ini} obtained at the end of the sample preparation are not affected by the values of n_{it}.

Finally, an isotropic compression setting the particle friction $\mu_{\mathrm{iso}} = \mu_{\mathrm{biax}} = 1$ is performed, where $\mu_{\mathrm{biax}} = 1$ is the particle friction considered during the multiaxial testing explained in the following.

Multiaxial loading configuration. An increase of the external axial stress σ_1 is prescribed to impose the constant axial strain rate (see below), whereas the radial stress σ_3, i.e., the confining pressure, is kept constant. The external mechanical loading is prescribed on the grain assembly, using periodic boundary conditions. Instead of considering a sample delimited by rigid walls on which force is applied at the boundary of the sample, which would lead to an inhomogeneous repartition of the external force through the granular assembly (16), we consider a periodic simulation cell.

The grain stiffness coefficient $k_t = k_n$ and the confining pressure σ_3 are sized with respect to the contact stiffness $K = k_n/\sigma_3$ that we set equal to 1,000. This value for K is of the order of the one obtained in a compression experiment performed on glass bead assemblies under 100 kPa of confining pressure, where K approximately equals 3,000 in that case.

The axial strain ε is imposed to increase at a constant rate by prescribing a constant strain increment $\delta\varepsilon_1$ at each discretization time interval. To ensure quasi-static loading, $\delta\varepsilon_1$ is sized with respect to the inertial number I defined as $I = \dot{\varepsilon}_1\sqrt{\overline{\mathbf{m}}/\sigma_3}$, where $\overline{\mathbf{m}}$ is the average grain mass. We here set $I = 5 \times 10^{-5}$, ensuring quasi-static loading (16, 19).

As for the multiaxial compression tests on coal discussed in Fig. 2, the deviatoric stress $\sigma_1 - \sigma_3$ has been considered here as the relevant variable.

Simulations. Simulations were performed for various sample sizes defined as $L = \sqrt{N_g}$. We made L to vary from 10 to 212. The number of independent simulations performed with each system size has been set equal to 100, except for the largest system size $L = 212$ for which only 20 simulations have been performed.

The sample preparation procedure described above is a way to set different levels of initial disorder, allowing us to check the robustness of our size-effect formalism against this disorder level. In other words, disorder is not introduced in an *ad hoc* manner, but rather has a topological origin that is physically materialized at the microscopic scale by changes in the spatial organization of grains and grain contacts. This initial topological disorder has a strong influence on macroscopic behavior: The HC samples appear much stiffer than LC samples, with a brutal postinstability softening. Despite these strongly different macroscopic responses, the size effects on yield stress are very well described by our formalism (Eqs. **1** and **2** of the main text) for HC, LC1, and LC2 samples, with an exponent ν_{FS} that is very close to 1 in all cases (Table S1), in agreement with the mean-field exponent ν of the depinning transition (20). On the contrary, the disorder plays a significant role on asymptotic strength, with a larger σ_∞ for highly coordinated, dense samples, as expected. The scales L_A and L_B are slightly larger than the average particle size and increase for less dense, less coordinated samples, as expected.

1. Fisher DS, Dahmen K, Ramanathan S, Ben-Zion Y (1997) Statistics of earthquakes in simple models of heterogeneous faults. *Phys Rev Lett* 78(25):4885–4888.
2. Gao HJ, Rice JR (1989) A first-order perturbation analysis of crack trapping by arrays of obstacles. *J Appl Mech Trans ASME* 56(4):828–836.
3. Charles Y, Hild F, Roux S, Vandembroucq D (2006) Material-independent crack arrest statistics: Application to indentation experiments. *Int J Fract* 142(1–2):51–67.
4. Patinet S, Vandembroucq D, Roux S (2013) Quantitative prediction of effective toughness at random heterogeneous interfaces. *Phys Rev Lett* 110(16):165507.
5. Talamali M, Petäjä V, Vandembroucq D, Roux S (2012) Strain localization and anisotropic correlations in a mesoscopic model of amorphous plasticity. *C R Mec* 340(4–5):275–288.
6. Eshelby JD (1957) The determination of the elastic field of an ellipsoidal inclusion, and related problems. *Proc R Soc A* 241:376–396.
7. Eshelby JD (1959) The elastic field outside an ellipsoidal inclusion. *Proc R Soc A* 252:561–569.
8. Gong SX, Meguid SA (1993) Interacting circular inhomogeneities in plane elastostatics. *Acta Mech* 99(1–4):49–60.
9. Jaeger JC, Cook NGW (1979) *Fundamentals of Rock Mechanics* (Chapman & Hall, London).
10. Sevostianov I, Kachanov M (2011) Elastic fields generated by inhomogeneities: Far-field asymptotics, its shape dependence and relation to the effective elastic properties. *Int J Solids Struct* 48(16–17):2340–2348.
11. Sevostianov I, Kachanov M (2012) Is the concept of "average shape" legitimate, for a mixture of inclusions of diverse shapes? *Int J Solids Struct* 49(23–24):3242–3254.
12. Roux S, Hild F (2002) On the relevance of mean field to continuum damage mechanics. *Int J Fract* 116(3):219–229.
13. Baret JC, Vandembroucq D, Roux S (2002) Extremal model for amorphous media plasticity. *Phys Rev Lett* 89(19):195506.
14. Girard L, Amitrano D, Weiss J (2010) Fracture as a critical phenomenon in a progressive damage model. *J Stat Mech* 2010:P01013.
15. Girard L, Weiss J, Amitrano D (2012) Damage-cluster distributions and size effect on strength in compressive failure. *Phys Rev Lett* 108(22):225502.
16. Radjai F, Dubois F (2011) *Discrete-Element Modelling of Granular Materials* (Wiley, Hoboken, NJ).
17. Gimbert F, Amitrano D, Weiss J (2013) Crossover from quasi-static to dense flow regime in compressed frictional granular media. ArXiv:1208.1930.v3.
18. Agnolin I, Roux JN (2007) Internal states of model isotropic granular packings. I. Assembling process, geometry, and contact networks. *Phys Rev E Stat Nonlin Soft Matter Phys* 76(6 Pt 1):061302.
19. GDR MiDi (2004) On dense granular flows. *Eur Phys J E Soft Matter* 14(4):341–365.
20. Ertas D, Kardar M (1994) Critical dynamics of contact line depinning. *Phys Rev E Stat Phys Plasmas Fluids Relat Interdiscip Topics* 49(4):R2532–R2535.

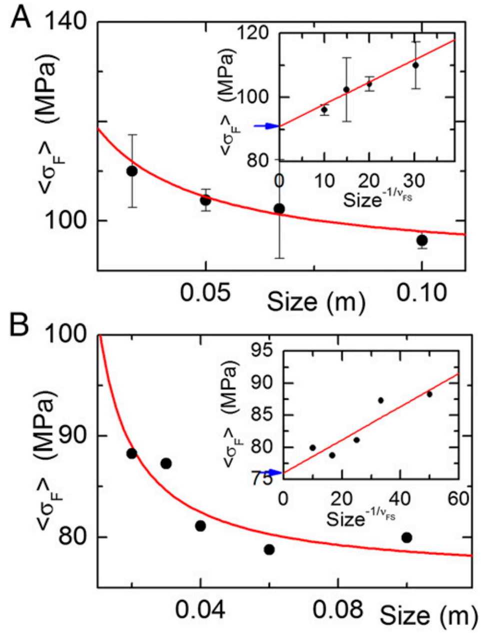

Fig. S1. (*A* and *B*) Finite-size effect on uniaxial compressive strength for HP concrete (1) (*A*) and marble (2) (*B*). Main graphs: mean compressive strength σ_f vs. size. Black circles: published experimental data, with associated SD (when reported). Red curve: fit by Eq. **3** of the main text, using $\nu_{FS} = 1$. The best-fit asymptotic strengths σ_∞ are 91 MPa for HP concrete and 76 MPa for marble. The associated scales L_B are, respectively, 7.6 mm and 3.4.mm. Insets show same data and fits, in a σ_f vs. $L^{-1/\nu_{FS}}$ graph, where Eq. **3** is a straight line and reveals the asymptotic strength σ_∞.

1. del Viso JR, Carmona JR, Ruiz G (2008) Shape and size effects on the compressive strength of high-strength concrete. *Cement Concr Res* 38:386–395.
2. Mogi K (1962) The influence of the dimensions of specimens on the fracture strength of rocks. *Bull Earthquake Res Inst* 40:175–185.

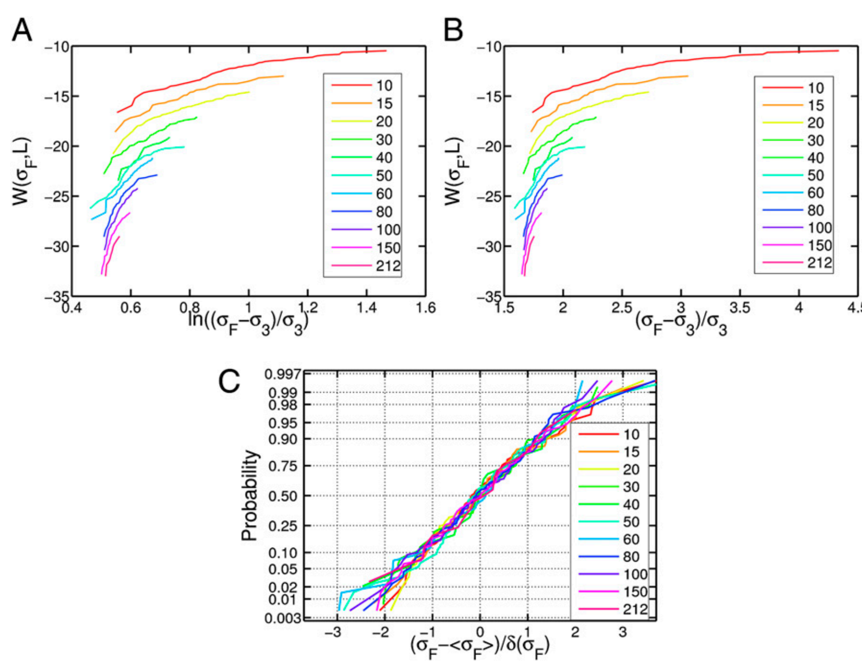

Fig. S2. Distribution of multiaxial compressive strength for the discrete-element model of frictional granular media (LC1 samples; details in *SI Text*). (*A* and *B*) Weibull (*A*) and Gumbel (*B*) statistics, where $W(L,\sigma_f) = \ln(-\ln(1 - P_F(\sigma))/L^2)$ and $P_F(\sigma)$ is the (cumulative) probability of failure under an applied stress σ. Because data obtained for different sample sizes do not collapse onto a single straight line, compressive strengths do not follow either Weibull or Gumbel statistics. (*C*) Normal probability plot for the standard distributions. The collapse onto a single straight line argues for Gaussian statistics.

Table S1. Parameters describing the initial properties of granular samples considered and the finite-size scaling of compressive strength

Sample type	ν_{FS}	A	B	L_A	L_B	σ_∞/σ_3	Φ_{ini}	Z^*_{ini}
HC	1.01	3.36	4.14	1.55	1.92	2.17	0.847 ± 0.001	4
LC1	1.07	2.68	6.32	1.68	4.21	1.65	0.847 ± 0.001	3 ± 0.1
LC2	1.03	2.13	5.52	2.27	6.06	0.96	0.819 ± 0.002	3 ± 0.1